Maximal coin-position entanglement generation in a quantum walk for the third step and beyond regardless of the initial state

Xiao-Xu Fang,[1] Kui An,[1] Bai-Tao Zhang,[2] Barry C. Sanders,[3] and He Lu[1,4,*]

[1]*School of Physics, State Key Laboratory of Crystal Materials, Shandong University, Jinan 250100, China*
[2]*State Key Laboratory of Crystal Materials, Institute of Novel Semiconductors, Shandong University, Jinan 250100, China*
[3]*Institute for Quantum Science and Technology, University of Calgary, Alberta, Canada T2N 1N4*
[4]*Shenzhen Research Institute of Shandong University, Shenzhen 518057, China*

(Received 11 October 2022; accepted 11 January 2023; published 30 January 2023)

We study maximal coin-position entanglement generation via a discrete-time quantum walk, in which the coin operation is randomly selected from one of two coin operators set at each step. We solve maximal entanglement generation as an optimization problem with quantum process fidelity as the cost function. Then we determine the maximal entanglement that can be rigorously generated for any step beyond the second regardless of initial conditions with appropriate coin sequences. The simplest coin sequence comprising Hadamard and identity operations is equivalent to the generalized elephant quantum walk, which exhibits an increasingly faster spreading in terms of probability distribution. Experimentally, we demonstrate a ten-step quantum walk driven by such coin sequences with linear optics and thereby show the desired high-dimensional bipartite entanglement as well as the transport behavior of faster spreading.

DOI: 10.1103/PhysRevA.107.012433

A quantum walk (QW) is the quantum version of a classical random walk [1,2]. Due to the principle of superposition in quantum mechanics, a QW gives rise to impressive applications in quantum information science, from quantum computing [3–6] to quantum simulation [7], and from implementing quantum measurement [8–10] to exploring topological phases [11–18]. For the discrete-time QW (DTQW), entanglement can be generated between coin and position degree of freedom of the walker, so called the coin-position entanglement [19–22], which is a key resource for quantum information processing [23]. The entangled states generated in DTQW are generally high-dimensional quantum states ($2 \otimes d$) that exhibit contents richer than those of qubit states ($2 \otimes 2$) [24]. Thus, DTQW provides an experimental platform to investigate quantum correlations of $2 \otimes d$ quantum states in terms of separability and entanglement detection [25–29], entanglement of formation [30,31], survival of entanglement [32,33], concurrence [34–36], and discord [37–39].

In a one-dimensional (1D) DTQW with static coin operations (unchanging coin operation during evolution), entanglement generation depends on the initial coin state and cannot reach the maximal value [19,20]. Counterintuitively, by introducing disorder into the DTQW [40], e.g., randomly choosing SU(2) coin operation

$$\hat{C}(\xi,\gamma,\zeta)=\begin{pmatrix} e^{i\xi}\cos\gamma & e^{i\zeta}\sin\gamma \\ e^{-i\zeta}\sin\gamma & -e^{-i\xi}\cos\gamma \end{pmatrix}, \quad 4\gamma,\xi,\zeta \in [0,2\pi], \tag{1}$$

at each step, generated entanglement is significantly enhanced and achieves maximal entanglement generation (MEG) asymptotically independent of initial conditions [41,42]. Motivated by robust entanglement generation under experimental conditions with imperfections and disorder, random-coin DTQWs have been theoretically studied for various disorder configurations [43–52] and have been experimentally observed with linear optics [53–55]. The enhancement of entanglement is not limited to the disorder in coin operation. Introducing the disorder in the shift operator can enhance the coin-position entanglement generation as well [56–59]. Besides, phenomena of entanglement boosting also exist in the quantum Parrondo walk [60–63].

The MEG with a fixed initial coin state can be obtained either in the asymptotic approach [56,57] or with specifically designed coin-operation sequences (henceforth called a coin sequence) [54,55,64]. MEG, regardless of initial coin states, is generally achieved in an asymptotic approach via QW with disorder either in coin operations [41] or in shift operations [59], which is problematic for current experimental technologies. Strategies to optimize coin sequences during the evolution have been proposed aiming at MEG for few steps. Universal coin sequences are proposed to generated highly entangled states for fewer than ten steps [65]. However, the universal sequence works for an odd number of steps and for the states with vanishing relative phase. Parrondo sequences have been proposed to generate maximal entanglement at steps $T = 3$ and $T = 5$ [66]. Ideal MEG via a DTQW should work for any step number *and* independent of initial conditions, but previous experiments have achieved either one or the other, not both; we achieve both simultaneously here for all steps beyond the second by solving an optimization problem. Interestingly, the determined optimal coin sequences are equivalent to the generalized elephant quantum walk (gEQW) [56,59], in which the spreading of the probability distribution

*luhe@sdu.edu.cn

 ©2023 American Physical Society

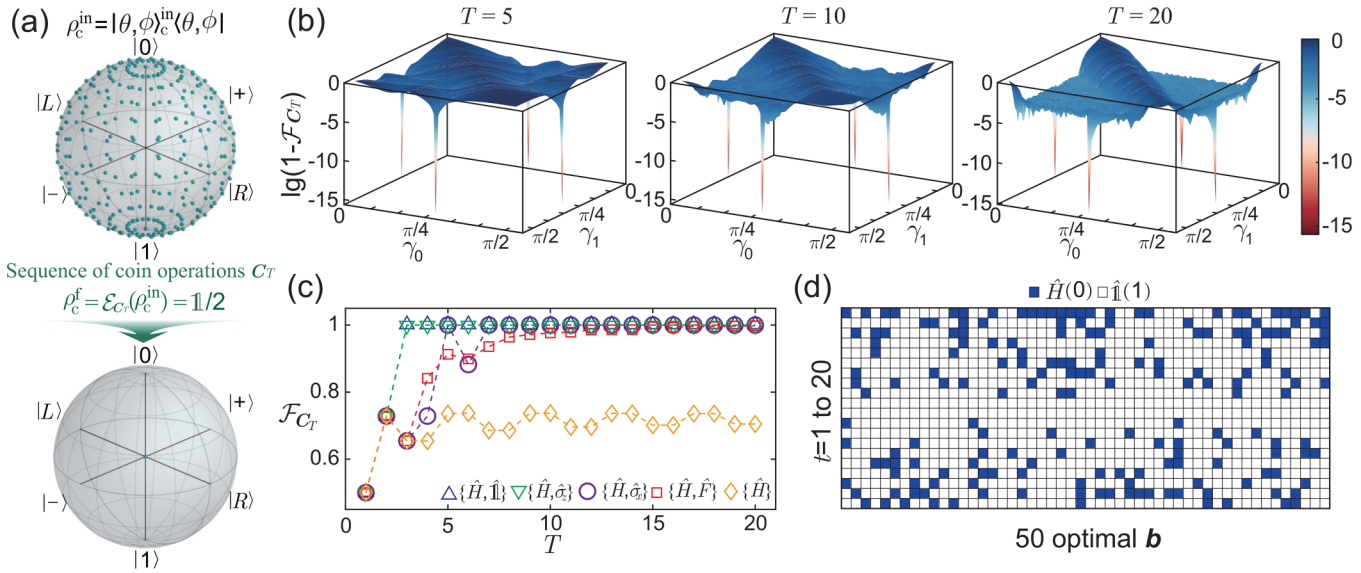

FIG. 1. (a) The geometric representation of the optimal coin sequence $\boldsymbol{C}_T$ that can generate maximal entanglement irrelevant of initial state $|\theta,\phi\rangle_{\rm c}^{\rm in}$. (b) Results of optimization of $1-\mathcal{F}_{\boldsymbol{C}_T}$ with $\hat{C}_t \in \{\hat{C}(\gamma_0), \hat{C}(\gamma_1)\}$ at $T=5$, $T=10$, and $T=20$. The values of $\gamma_{(0,1)}$ are taken from 0° to 90° with an interval of 1°. (c) The maximal $\mathcal{F}_{\boldsymbol{C}_T}$ in a QW from $T=1$ to $T=20$ with coin set $\{\hat{H},\hat{\mathbb{1}}\}$ (blue up-pointing triangle), $\{\hat{H},\hat{\sigma}_z\}$ (green down-pointing triangle), $\{\hat{H},\hat{\sigma}_x\}$ (purple circle), $\{\hat{H},\hat{F}\}$ (red square), and $\{\hat{H}\}$ (yellow diamond). (d) Fifty $\boldsymbol{b}$'s that can achieve $\mathcal{F}_{\boldsymbol{C}_T}=1$ at $T=20$ with coin set $\{\hat{H},\hat{\mathbb{1}}\}$, where 0 represents $\hat{H}$ and 1 represents $\hat{\mathbb{1}}$.

is much faster. Experimentally, we demonstrate the DTQW with requisite coin sequences up to ten steps with linear optics and observe significant enhancement of entanglement generation as well as spreading behavior compared to other schemes.

In the 1D DTQW, the Hilbert space of coin (c) and position (p) of the walker is $\mathscr{H}=\mathscr{H}_{\rm c}\otimes\mathscr{H}_{\rm p}$, with

$$\mathscr{H}_{\rm c}=\text{span}\{|0\rangle_{\rm c},|1\rangle_{\rm c}\},\quad \mathscr{H}_{\rm p}=\text{span}\{|x\rangle_{\rm p};x\in\mathbb{Z}\}. \tag{2}$$

The walker is initially localized in position state $|0\rangle_{\rm p}$, with arbitrary initial coin $|\theta,\phi\rangle_{\rm c}^{\rm in}=\cos(\theta/2)|0\rangle_{\rm c}+e^{i\phi}\sin(\theta/2)|1\rangle_{\rm c}$, where $2\theta,\phi\in[0,2\pi]$. At step t, the coin operator $\hat{C}_t$ is applied. Then the walker moves left or right conditioned on the coin state by

$$\hat{S}=\sum_x |x+1\rangle_{\rm p}\langle x|\otimes|0\rangle_{\rm c}\langle 0|+|x-1\rangle_{\rm p}\langle x|\otimes|1\rangle_{\rm c}\langle 1|, \tag{3}$$

which is independent of t.

For $t\in[N]=\{1,\ldots,N\}$, the evolution is

$$|\theta,\phi\rangle_{\rm f}=\prod_{t\in[T]}\hat{U}_t|\theta,\phi\rangle_{\rm c}^{\rm in}\otimes|0\rangle_{\rm p},\quad \hat{U}_t=\hat{S}(\hat{C}_t\otimes\hat{\mathbb{1}}_{\rm p}), \tag{4}$$

where $\hat{\mathbb{1}}_{\rm p}=\sum_x|x\rangle\langle x|$ is the identity operator on $\mathscr{H}_{\rm p}$, and "f" is short for "final." The sequence $\boldsymbol{C}_T=(\hat{C}_t)_{t\in[T]}$ describes coin operations applied to the walker.

Achieving coin-position MEG at step T regardless of $|\theta,\phi\rangle_{\rm c}^{\rm in}$ corresponds to designing $\boldsymbol{C}_T$ that maps any $|\theta,\phi\rangle_{\rm c}^{\rm in}\otimes|0\rangle_{\rm p}$ to the maximally entangled coin-position state $|\theta,\phi\rangle_{\rm f}$. Entanglement of $|\theta,\phi\rangle_{\rm f}$ is quantified by the Von Neumann entropy,

$$\mathcal{S}_{\rm E}(|\theta,\phi\rangle_{\rm f})=-\text{tr}\big(\rho_{\rm c}^{\rm f}\log_2\rho_{\rm c}^{\rm f}\big)=-\sum_{\varepsilon\in\pm}\lambda_\varepsilon\log_2\lambda_\varepsilon, \tag{5}$$

of the reduced coin state [20,67], where $\rho_{\rm c}^{\rm f}=\text{tr}_{\rm p}(|\theta,\phi\rangle_{\rm f}\langle\theta,\phi|)$ and $\lambda_\pm$ are the eigenvalues of $\rho_{\rm c}^{\rm f}$. Note that $0\leqslant\mathcal{S}_{\rm E}\leqslant 1$, and $\mathcal{S}_{\rm E}\equiv 0$ for separable states and 1 for maximally entangled states.

Thus, MEG evolution (4) yields maximally entangled $|\theta,\phi\rangle_{\rm f}$, which is equivalent to $\mathcal{E}_{\boldsymbol{C}_T}(\rho_{\rm c}^{\rm in}=|\theta,\phi\rangle_{\rm c}^{\rm in}\langle\theta,\phi|)=\mathbb{1}/2$ in $\mathscr{H}_{\rm c}$, where $\mathcal{E}_{\boldsymbol{C}_T}$ is a completely positive linear map determined by $\boldsymbol{C}_T$. A geometric illustration of $\mathcal{E}_{\boldsymbol{C}_T}$ for MEG is in Fig. 1(a), which is the depolarizing channel $\mathcal{E}^{\rm DP}(\rho_{\rm c}^{\rm in})=(1-\eta)\rho_{\rm c}^{\rm in}+\eta\frac{\mathbb{1}}{2}$ with $\eta=1$ [68]. Process fidelity $\mathcal{F}_{\boldsymbol{C}_T}=\text{tr}(\sqrt{\sqrt{\chi_{\boldsymbol{C}_T}}\chi_{\rm DP}\sqrt{\chi_{\boldsymbol{C}_T}}})^2$ [69,70] is our figure of merit to design $\boldsymbol{C}_T$, where $\chi_{\boldsymbol{C}_T}$ is the Pauli-matrix representation of the quantum channel $\mathcal{E}_{\boldsymbol{C}_T}$. Note that $\mathcal{F}_{\boldsymbol{C}_T}=1$ indicates MEG at step T regardless of $|\theta,\phi\rangle_{\rm c}^{\rm in}$, and we refer to the corresponding coin sequence $\boldsymbol{C}_T$ as the *optimal* coin sequence. In this sense, the design of optimal $\boldsymbol{C}_T$ can be addressed by solving the optimization problem

$$\begin{aligned}&\text{maximize}\quad \mathcal{F}_{\boldsymbol{C}_T}=\text{tr}(\sqrt{\sqrt{\chi_{\boldsymbol{C}_T}}\chi_{\rm DP}\sqrt{\chi_{\boldsymbol{C}_T}}})^2\\ &\text{subject to}\quad \hat{C}_t\in\text{SU}(2).\end{aligned} \tag{6}$$

A general SU(2) coin operation in Eq. (1) has three parameters, which makes the optimization rather resource demanding. To simplify the optimization, we replace $\hat{C}(\gamma)\leftarrow\hat{C}(0,\gamma,0)$. Furthermore, we restrict construction of $\boldsymbol{C}_T$ by allowing only two coin operations, i.e., $\gamma_{0,1}$ labeled by one bit with values 0 and 1. Then the optimization Eq. (6) converts to

$$\begin{aligned}&\text{maximize}\quad \mathcal{F}_{\boldsymbol{C}_T}=\text{tr}(\sqrt{\sqrt{\chi_{\boldsymbol{C}_T}}\chi_{\rm DP}\sqrt{\chi_{\boldsymbol{C}_T}}})^2\\ &\text{subject to}\quad \hat{C}_t\in\{\hat{C}(\gamma_0),\hat{C}(\gamma_1)\},\quad \gamma_{0,1}\in[0,\pi/2].\end{aligned} \tag{7}$$

We solve optimization (7) using an annealing algorithm. The results of optimization of $\gamma_{0,1}$ at $T\in\{5,10,20\}$ are

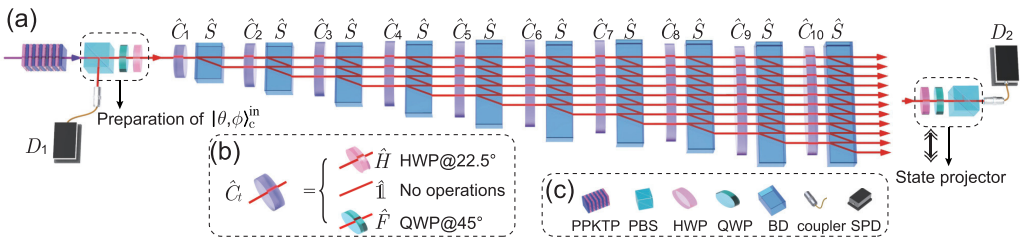

FIG. 2. (a) Detailed sketch of the setup to realize the ten-step DTQW. (b) Coin operations realized in experiment. A half-wave plate (HWP) set at 22.5° corresponds to operation $\hat{H}$ and a quarter-wave plate (QWP) set at 45° corresponds to operation $\hat{F}$. No wave plate needs to be arranged if the operation is $\mathbb{1}$. (c) Symbols used in panels (a) and (b): periodically poled potassium titanyl phosphate, PPKTP; polarization beam splitter, PBS; half-wave plate, HWP; quarter-wave plate, QWP; beam displacer, BD; and single photon detector, SPD.

shown in Fig. 1(b). Evidently, the minimal $1-\mathcal{F}_{\boldsymbol{C}_T}$ is obtained for two coin sets: $\{\hat{C}(0),\hat{C}(\pi/4)\}$ and $\{\hat{C}(\pi/2),\hat{C}(\pi/4)\}$. Note that $\hat{C}(0)=\hat{\sigma}_z$, $\hat{C}(\pi/4)=\hat{H}$, and $\hat{C}(\pi/2)=\hat{\sigma}_x$. The evolution unitary operator with the coin operator $\hat{\sigma}_z$, i.e., $\hat{U}=\hat{S}\hat{\sigma}_z$, makes the components $|0\rangle_c$ and $|1\rangle_c$ propagate in the opposite direction without interference, which has the similar effect of $\hat{U}=\hat{S}\mathbb{1}$. The difference is that $\hat{\sigma}_z$ delivers a phase π ($e^{i\pi}=-1$) on component $|1\rangle_c$ while $\mathbb{1}$ delivers zero phase ($e^{i0}=1$), which does not affect the amount of entanglement of the final state. Along this spirit, we conjecture that the coin set $\{\hat{H},\mathbb{1}\}$ is as effective as $\{\hat{H},\hat{\sigma}_z\}$ in terms of MEG. To confirm this conjecture, we solve Eq. (7) by restricting $\hat{C}_t\in\{\hat{H},\mathbb{1}\}$ and $\hat{C}_t\in\{\hat{H},\hat{\sigma}_z\}$, respectively, and the results of optimized $\mathcal{F}_{\boldsymbol{C}_T}$ with T up to 20 are shown with blue up-pointing triangles and green down-pointing triangles in Fig. 1(c).

We observe that optimized $\mathcal{F}_{\boldsymbol{C}_T}$ values with these two coin sets are exactly same, in which $\mathcal{F}_{\boldsymbol{C}_T}=1$ since step $T=3$. To give a comparison, we also show the optimized $\mathcal{F}_{\boldsymbol{C}_T}$ with coin sets $\{\hat{H},\hat{\sigma}_x\}$ and $\{\hat{H}\}$. We also consider the coin set of $\{\hat{H},\hat{F}\}$ with $\hat{F}=[1,i;i,1]/\sqrt{2}$ being the Kempe coin operator [2], which is widely adopted in the investigation of entanglement generation in discorded QW [41,48,53,65]. As shown in Fig. 1(c), $\mathcal{F}_{\boldsymbol{C}_T}=1$ is achieved at step $T=5$ and $T\geqslant 7$ for the coin set $\{\hat{H},\hat{\sigma}_x\}$ (purple circles). Asymptomatic behavior is observed with the coin set $\{\hat{H},\hat{F}\}$ (red squares) and oscillating behavior is observed in the Hadamard walk (yellow diamonds). The optimized $\mathcal{F}_{\boldsymbol{C}_T}$ is associated with a bit string $\boldsymbol{b}\in\{0,1\}^T$ of length T with 0 labeling $C(\gamma_0)$ and 1 labeling $C(\gamma_1)$. We note that optimal $\boldsymbol{b}$ at step T is not unique. For instance, we obtain 1104 optimal $\boldsymbol{b}$ with the coin set $\{\hat{H},\mathbb{1}\}$ at $T=20$, and we list 50 among them in Fig. 1(d). There are no obvious features of regularities and generalities of these optimal $\boldsymbol{b}$'s. An optimal $\boldsymbol{b}$ containing 0 ($\hat{H}$) as little as possible is preferred in experiment. Considering the spreading behavior with the optimal coin sequences, we experimentally choose the optimal $\boldsymbol{b}$ containing two or three 0s in our realization. (The explicit form of $\boldsymbol{b}$ and its corresponding proof are given in Appendix A) Note that the optimal $\boldsymbol{b}$ generally guarantees the MEG at step T. However, there indeed exists optimal $\boldsymbol{b}$, such as the sequences in Appendix A, which leads to MEG at intermediate steps as well.

In fact, the disordered QW with the coin set $\{\hat{H},\mathbb{1}\}$ is equivalent to the gEQW [56,59], which is a QW with disorder in the shift operator. In gEQW, the coin operator is step independent (static coin), and the shift operator is step dependent according to

$$\hat{S}_{\mathrm{gEQW}}(\Delta_t)=\sum_x |x+\Delta_t\rangle_p\langle x|\otimes|0\rangle_c\langle 0|+|x-\Delta_t\rangle_p\langle x|\otimes|1\rangle_c\langle 1|, \tag{8}$$

with $\Delta_t\in[1,2,\ldots,T]$. The probability distribution of Δ_t is a discretized version of the q-exponential distribution [71]. As a consequence, the case of $q=0.5$ corresponds to a standard Hadamard QW, while for $q\to\infty$ the shift operation Eq. (8) becomes completely disordered.

In our model, the evolution of the l-step QW with a coin sequence comprised of a single Hadamard operation followed by $l-1$ identity operations corresponds to a one-step gEQW with $\Delta_t=l$:

$$\prod_{\boldsymbol{b}=01\cdots 1}\hat{S}(\hat{C}_t\otimes\mathbb{1}_p)=\hat{S}_{\mathrm{gEQW}}(\Delta_1=l)\hat{H}\otimes\mathbb{1}_p. \tag{9}$$

For instances, the optimal $\boldsymbol{b}$ in the first column of Fig. 1(d) is $\boldsymbol{b}=01111111110101111011$, which corresponds to a four-step gEQW with $\Delta_1=11$, $\Delta_2=2$, $\Delta_3=4$, and $\Delta_4=3$ (See Appendix B for more details). Compared to the QW with disorder in the coin operation, the gEQW exhibits a faster spreading while maintaining the capability of asymptotic MEG [56,59].

We implement the 1D DTQW with the well-established dynamical evolution of a single photon in a linear optical network [72–74]. The experimental setup is shown in Fig. 2(a). The coin state is encoded in the photon's polarization degree of freedom by $|H(V)\rangle=|0(1)\rangle$, where $|H(V)\rangle$ denotes the horizontal (vertical) polarization. The position state is encoded in the photon's spatial degree of freedom, i.e., the transverse spatial modes. Two photons in state $|H\rangle|V\rangle$ with a central wavelength at 810 nm are generated from a periodically poled potassium titanyl phosphate (PPKTP) crystal pumped by an ultraviolet continuous-wave laser diode with the central wavelength at 405 nm [75–77].

During our experiment, the count rate of two-photon coincidences is about 2.8×10^4/s with a pump power of 10 mW. The two photons are then separated by a polarizing beam splitter (PBS), which transmits the horizontal polarization and reflects vertical polarization. The reflected photon is detected by a single-photon detector (SPD) to serve as a trigger. The transmitted photon is sent into the photonic network consisting of wave plates and birefringent calcite beam

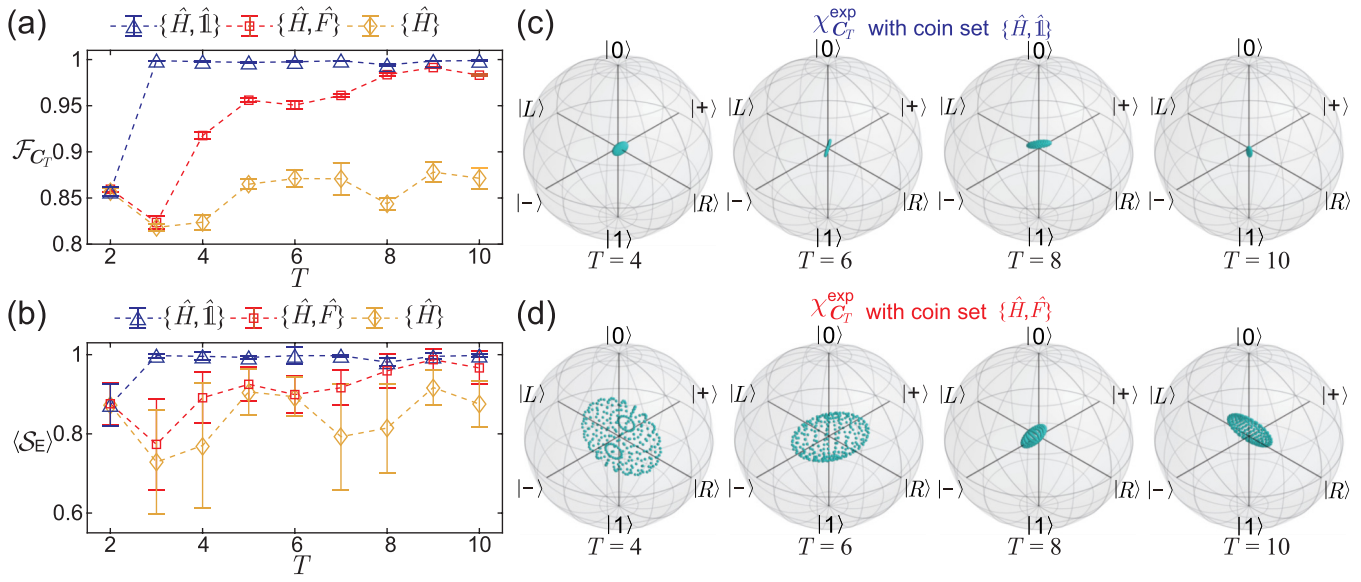

FIG. 3. (a) Experimental results of $\mathcal{F}_{\boldsymbol{C}_T}$ with coin sets $\{\hat{H},\hat{\mathbb{1}}\}$ (blue up-pointing triangles), $\{\hat{H},\hat{F}\}$ (red squares), and $\{\hat{H}\}$ (yellow diamonds) at $T=2$ to $T=10$. (b) Average entanglement $\langle\mathcal{S}_{\mathrm{E}}\rangle$ over 296 initial coin states with the reconstructed $\chi^{\mathrm{exp}}_{\boldsymbol{C}_T}$. (c) Geometric representation of reconstructed $\chi^{\mathrm{exp}}_{\boldsymbol{C}_T}$ with the coin set $\{\hat{H},\hat{\mathbb{1}}\}$ at $T=4$, 6, 8, and 10. (d) Geometric representation of reconstructed $\chi^{\mathrm{exp}}_{\boldsymbol{C}_T}$ with the coin set $\{\hat{H},\hat{F}\}$ at $T=4$, 6, 8, and 10.

displacers (BDs), in which the longitudinal spatial mode of the injected photon is denoted as the start position of the walker $|0\rangle_{\mathrm{p}}$. The coin operations $\hat{C}_t$ are realized by wave plates which rotate the polarization of the photon, and the BD transmits the vertical polarization while deviating from the horizontal polarization so that the BD acts as the shift operation $\hat{S}$.

By carefully adjusting the position between any pair of two BDs, we observe an average interference visibility beyond 0.99. Note that if no wave plate is set between two BDs, the concatenation of two BDs corresponds to the shift operator (8) with $\Delta_t=2$. The outgoing state is detected by a state analyzer as shown in Fig. 2(a). The projective measurement on the position state $|x\rangle$ is achieved by placing a SPD at the corresponding output mode of the optical network, and the projective measurement on an arbitrary coin state is implemented by a HWP, a QWP, and a PBS.

To reconstruct the process matrix $\chi^{\mathrm{exp}}_{\boldsymbol{C}_T}$, we prepare four states as initial coin states $|\theta,\phi\rangle^{\mathrm{in}}_{\mathrm{c}}$, i.e., $|H\rangle$, $|V\rangle$, $|+\rangle=1/\sqrt{2}(|0\rangle+|1\rangle)$ and $|L\rangle=1/\sqrt{2}(|0\rangle+i|1\rangle)$. For each step T, we set the optimal coin sequence $\boldsymbol{C}_T$ accordingly (see Appendix A for the settings of coin sequences), and we reconstruct $\rho^{\mathrm{f}}_{\mathrm{c}}$ using quantum-state tomographic technology [68]. To this end, we first set the measurement apparatus at one mode of the output of the optical network, and we perform the projective measurement on coin states $|H\rangle$, $|V\rangle$, $|+\rangle$, and $|L\rangle$, respectively. Then we move the measurement apparatus to the next optical mode and repeat the process of projective measurements aforementioned.

After collecting the data over all optical modes, we put the data together to perform quantum-state tomography without distinguishing which mode they come from, which corresponds to trace out of position DOF. Roughly 2.2×10^5 two-photon coincidences are collected to perform process tomography at each step. The experimental results of $\mathcal{F}_{\boldsymbol{C}_T}$ with the coin set $\{\hat{H},\hat{\mathbb{1}}\}$ are shown with blue triangles in Fig. 3(a). We observe that the average $\mathcal{F}_{\boldsymbol{C}_T}$ from $T=3$ to $T=10$ is 0.9954 ± 0.0008, which is much better than the results with the coin set $\{\hat{H},\hat{F}\}$ as shown with red squares. For the Hadamard QW, $\mathcal{F}_{\boldsymbol{C}_T}<0.8$ and oscillates as T increases (shown with yellow diamonds). We calculate the average entanglement $\langle\mathcal{S}_{\mathrm{E}}\rangle$ over 296 initial coin states with the reconstructed $\chi^{\mathrm{exp}}_{\boldsymbol{C}_T}$, and the results are shown in Fig. 3(b). The error bar indicates initial-state independence, and we observe a stronger initial-state independence with the coin set $\{\hat{H},\hat{\mathbb{1}}\}$ than with the other two. This is also reflected by the geometric interpretations of $\mathcal{F}_{\boldsymbol{C}_T}$ as shown in Fig. 3(c) (coin set $\{\hat{H},\hat{\mathbb{1}}\}$) and Fig. 3(d) (coin set $\{\hat{H},\hat{F}\}$) at $T=4$, 6, 8, and 10, respectively. It is obvious that the results with $\{\hat{H},\hat{\mathbb{1}}\}$ are much more dense than the results with $\{\hat{H},\hat{F}\}$, which indicates the entanglement generation with the coin set $\{\hat{H},\hat{\mathbb{1}}\}$ has independence of the initial coin states stronger than that with the other two. More details are shown in Appendix C.

We investigate the spreading properties of the demonstrated QW. We first investigate the uniformity of the probability distribution $\mathcal{P}(x,T)$ at step T, which can be characterized by the normalized Shannon entropy

$$\mathcal{S}_{\mathrm{S}}(T)=\frac{-\sum_x\mathcal{P}(x,T)\ln\mathcal{P}(x,T)}{\ln(T+1)},\tag{10}$$

with $1/\ln(T+1)$ being the normalization parameter. The walker is able to occupy $T+1$ positions after t steps so that the maximal value of $-\sum_x\mathcal{P}(x,T)\ln\mathcal{P}(x,T)$ is $\ln(T+1)$, which corresponds to the uniform distribution over $T+1$ positions [78]. Larger $\mathcal{S}_{\mathrm{S}}(T)$ implies $\mathcal{P}(x,T)$ is more uniform. For a T-step QW associated with the corresponding optimal $\boldsymbol{C}_T$, we measure the probability distribution $\mathcal{P}(x,T)$ at step T, according to which we calculate the normalized Shannon entropy $\mathcal{S}_{\mathrm{S}}(T)$. The results of $\mathcal{P}(x,T)$ with the initial coin

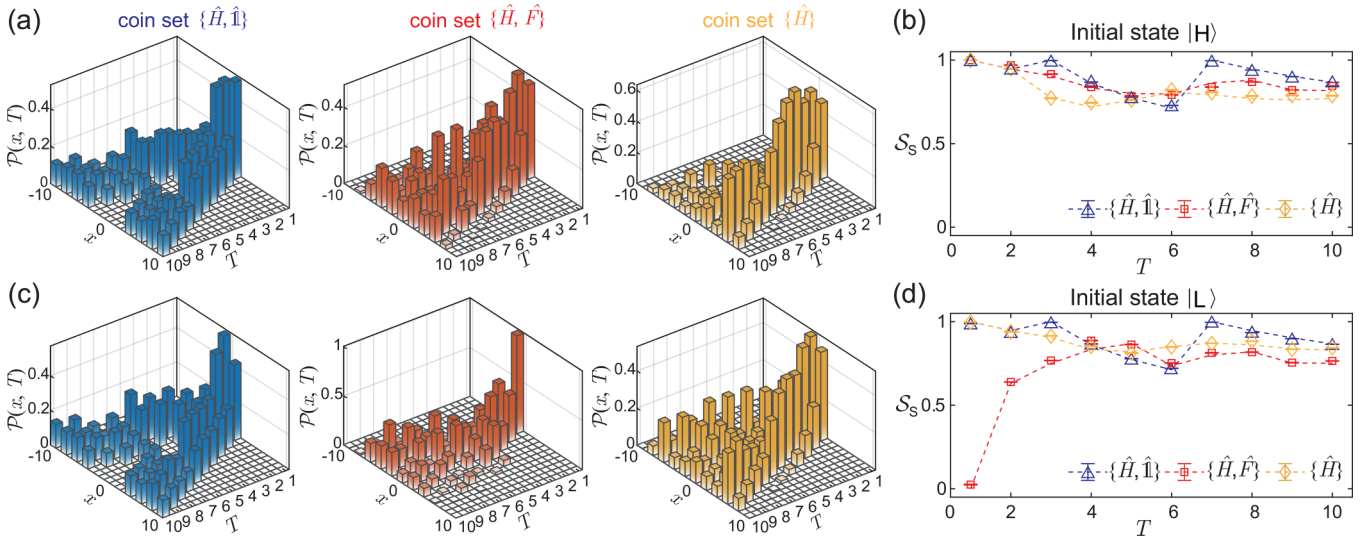

FIG. 4. Measured $\mathcal{P}(x, T)$ with initial coin states (a) $|H\rangle$ and (c) $|L\rangle$ driven by the coin sequences with coin sets $\{\hat{H}, \hat{\mathbb{1}}\}$, $\{\hat{H}, \hat{F}\}$, and $\{\hat{H}\}$, respectively. The calculated $\mathcal{S}_S(T)$ with measured $\mathcal{P}(x, T)$ of input states (b) $|H\rangle$ and (d) $|L\rangle$, where the results of coin sets $\{\hat{H}, \hat{\mathbb{1}}\}$, $\{\hat{H}, \hat{F}\}$, and $\{\hat{H}\}$ are shown with blue up-pointing triangles, red squares, and yellow diamonds, respectively.

states $|H\rangle$ and $|L\rangle$ are shown in Figs. 4(a) and 4(c), and the corresponding $\mathcal{S}_S(T)$ values are shown in Figs. 4(b) and 4(d), respectively. Compared with the other two cases, the uniformity of the QW with the coin set $\{\hat{H}, \hat{\mathbb{1}}\}$ is enhanced at $T = 3$ and $T = 7$. We also investigate the trend of probability distributions, which can be indicated by the second moment of the walker:

$$m(t) = \sum_x x^2 \mathcal{P}(x, t). \tag{11}$$

The walker shows a ballistic behavior if $m(t) \propto t^2$, while it shows a diffusive behavior if $m(t) \propto t$. Moreover, $m(t) \propto t^\alpha$ with $1 < \alpha < 2$ indicates a superdiffusive behavior [79]. Figure 5(a) shows the results of average $m(t)$ with the initial coin states $|H\rangle$, $|V\rangle$, $|+\rangle$, and $|L\rangle$ in a ten-step QW with three different coin sets. We observe that QWs with three coin sets spread faster than the classical random walk [$m(t) \propto t$]. We simulate 1000 QW with the coin operation randomly selected from the coin set $\{\hat{H}, \hat{\mathbb{1}}\}$, and the results of $m(t)$ are shown in Fig. 5(b). Asymptotically, the QW with the coin set $\{\hat{H}, \hat{\mathbb{1}}\}$ exhibits superdiffusive behavior as $m(t) \propto t^{1.47}$, which is slower than the ballistic behavior [$m(t) \propto t^2$] in the Hadamard walk [80]. However, for smaller t ($t \leqslant 10$), the QW with most fixed $\boldsymbol{C}_T$ spreads faster than the Hadamard walker as shown in the insert of Fig. 5(b). This is the reason why we observe the QW with the coin set $\{\hat{H}, \hat{\mathbb{1}}\}$ spreads faster than the Hadamard walk in our experiment ($T = 10$) as shown in Fig. 5(a).

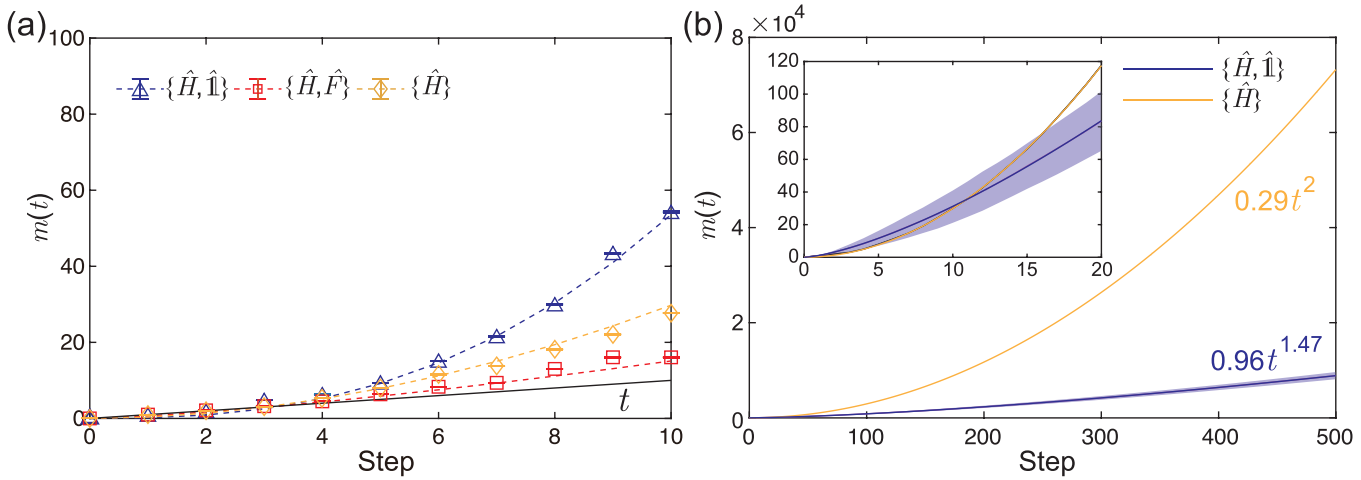

FIG. 5. (a) The experimental results of the second moment $m(t)$ in a ten-step QW. The blue up-pointing triangles represent the results with the coin set $\{\hat{H}, \hat{\mathbb{1}}\}$. The red squares and yellow diamonds represent the results with the coin sets $\{\hat{H}, \hat{F}\}$ and $\{\hat{H}\}$, respectively. The black line is $m(t) = t$. (b) The simulated 500-step QW with the coin sets $\{\hat{H}, \hat{\mathbb{1}}\}$ and $\{\hat{H}\}$. For QW with the coin set $\{\hat{H}, \hat{\mathbb{1}}\}$, the coin operation is randomly selected from the coin set $\{\hat{H}, \hat{\mathbb{1}}\}$ at each step. The average of $m(t)$ (blue line) is calculated on a sample of 1000 different $\boldsymbol{C}_T$ values, and the blue shade corresponds to the standard deviation of $m(t)$. The insert is $m(t)$ from $t = 1$ to $t = 20$.

In conclusion, we design coin sequences that can rigorously generate maximal entanglement between the coin and the position of the walker in a 1D DTQW with the following three key features: to be available at any $T \geqslant 3$, to be independent of initial coin state, and to be the simplest for experimental implementation. A comparison of our coin sequence $\boldsymbol{C}_T$ with the other coin sequences is shown in Appendix D, and MEG with our coin sequence significantly outperforms all other proposed coin sequences in the three features mentioned above. The QW with proposed coin sequences is equivalent to gEQW, which exhibits faster spreading.

Experimentally, we realize a ten-step 1D DTQW with proposed coin sequences, and we observe the entanglement generation as well as spreading behaviors. The results show a significant enhancement in terms of the entanglement generation, which benefits the intermediate quantum information processing that requires maximal qubit-qudit entanglement. Moreover, the spreading of probability distributions with our coin sequence reflects a higher uniformity and faster speedup, which is favorable and useful in various quantum algorithms and in quantum simulation of biological processes [78,81,82]. Our protocol can also be generalized to a p-diluted disordered QW [83,84], in which transport behavior can be engineered by controlling the probability of coin operations. As our model is equivalent to gEQW [56,59], a hyperballistic speedup is expected while maintaining the maximal entanglement generation.

We are grateful to two anonymous referees for providing very useful comments on earlier versions of this article. This work is supported by the Shandong Provincial Natural Science Foundation (Grants No. ZR2019MA001 and No. ZR2020JQ05), the National Natural Science Foundation of China (Grants No. 11974213 and No. 92065112), the National Key R&D Program of China (Grant No. 2019YFA0308200), Taishan Scholar of Shandong Province (Grant No. tsqn202103013), Shenzhen Fundamental Research Program (Grant No. JCYJ20190806155211142), Shandong University Multidisciplinary Research and Innovation Team of Young Scholars (Grant No. 2020QNQT), and the Higher Education Discipline Innovation Project ('111') (Grant No. B13029).

APPENDIX A: MEG WITH OPTIMAL COIN SEQUENCE

1. Fourier analysis of quantum walks

We use Fourier analysis to analyze the dynamical evolution in DTQW [85–88], which is defined as

$$|k\rangle = \sum_{x\in\mathbb{Z}} e^{ikx}|x\rangle, \quad |x\rangle = \int_{-\pi}^{\pi} \frac{dk}{2\pi} e^{-ikx}|k\rangle. \tag{A1}$$

With a Fourier transformation, the shift operator in Eq. (3) can be expressed in momentum space as

$$\begin{aligned}\hat{S}_{\mathrm{m}} &= (e^{-ik}|0\rangle\langle 0| + e^{ik}|1\rangle\langle 1|) \otimes |k\rangle\langle k| \\ &= \begin{pmatrix} e^{-ik} & 0 \\ 0 & e^{ik} \end{pmatrix} \otimes |k\rangle\langle k|. \end{aligned} \tag{A2}$$

Accordingly, the evolution unitary operator $\hat{U} = \hat{S}(\hat{C} \otimes \hat{\mathbb{1}}_{\mathrm{p}})$ is expressed by

$$\begin{aligned}\hat{U}_{\mathrm{m}} &= \hat{S}_{\mathrm{m}}(\hat{C} \otimes \hat{\mathbb{1}}_{\mathrm{p}}) \\ &= \begin{pmatrix} e^{-ik} & 0 \\ 0 & e^{ik} \end{pmatrix} \hat{C} \otimes |k\rangle\langle k| \sum_x |x\rangle\langle x| \\ &= \frac{1}{4\pi^2} \int dk \int dk' \begin{pmatrix} e^{-ik} & 0 \\ 0 & e^{ik} \end{pmatrix} \hat{C} \otimes \sum_x e^{-i(k-k')x} |k\rangle\langle k'| \\ &= \frac{1}{2\pi} \int dk \begin{pmatrix} e^{-ik} & 0 \\ 0 & e^{ik} \end{pmatrix} \hat{C} \otimes |k\rangle\langle k| \\ &= \int \hat{C}_{\mathrm{m}} \otimes \frac{dk}{2\pi} |k\rangle\langle k|, \end{aligned} \tag{A3}$$

where we have used the orthonormalization relation

$$\sum_{x\in\mathbb{Z}} e^{-i(k-k')x} = 2\pi\delta(k-k'), \tag{A4}$$

and we denote $\begin{pmatrix} e^{-ik} & 0 \\ 0 & e^{ik} \end{pmatrix}\hat{C}$ as $\hat{C}_{\mathrm{m}}$. Specifically, for the coin operations $\hat{C} = \hat{H}$ and $\hat{C} = \hat{\mathbb{1}}$, we obtain

$$\hat{H}_{\mathrm{m}} = \frac{1}{\sqrt{2}} \begin{pmatrix} e^{-ik} & e^{-ik} \\ e^{ik} & -e^{ik} \end{pmatrix}, \quad \hat{\mathbb{1}}_{\mathrm{m}} = \frac{1}{\sqrt{2}} \begin{pmatrix} e^{-ik} & 0 \\ 0 & e^{ik} \end{pmatrix}. \tag{A5}$$

Thus, the dynamic evolution of the initial state $|\theta,\phi\rangle_{\mathrm{c}}^{\mathrm{in}} \otimes |0\rangle_{\mathrm{p}}$ is

$$\begin{aligned}|\theta,\phi\rangle_{\mathrm{f}} &= \iint \prod_{t=1}^{T} \hat{C}_{\mathrm{m},t} \otimes \frac{dk}{2\pi} |k\rangle\langle k| \cdot |\theta,\phi\rangle_{\mathrm{c}}^{\mathrm{in}} \otimes \frac{dk'}{2\pi} |k'\rangle \\ &= \int \prod_{t=1}^{T} \hat{C}_{\mathrm{m},t} |\theta,\phi\rangle_{\mathrm{c}}^{\mathrm{in}} \otimes \frac{dk}{2\pi} |k\rangle. \end{aligned} \tag{A6}$$

The reduced density matrix of the coin is

$$\begin{aligned}\rho_{\mathrm{c}}^{\mathrm{f}} &= \mathrm{tr}_{\mathrm{p}}(|\theta,\phi\rangle_{\mathrm{f}}\langle\theta,\phi|) \\ &= \iint \sum_{x\in\mathbb{Z}} \prod_{t=1}^{T} \hat{C}_{\mathrm{m},t} |\theta,\phi\rangle_{\mathrm{c}}^{\mathrm{in}} \langle\theta,\phi| \hat{C}_{\mathrm{m},t}^{\dagger} \frac{dkdk'}{4\pi^2} \langle x|k\rangle\langle k'|x\rangle \\ &= \int \frac{dk}{2\pi} \prod_{t=1}^{T} \hat{C}_{\mathrm{m},t} |\theta,\phi\rangle_{\mathrm{c}}^{\mathrm{in}} \langle\theta,\phi| \hat{C}_{\mathrm{m},t}^{\dagger} \end{aligned} \tag{A7}$$

2. Superoperator

We describe the evolution acting on the coin state by a superoperator $\hat{\mathcal{L}}$:

$$\rho_{\mathrm{c}}^{t+1} = \hat{\mathcal{L}} \rho_{\mathrm{c}}^{t}. \tag{A8}$$

According to Eq. (A7), the one-step evolution is

$$\rho_{\mathrm{c}}^{t+1} = \int \frac{dk}{2\pi} \hat{C}_{\mathrm{m}} \rho_{\mathrm{c}}^{t} \hat{C}_{\mathrm{m}}^{\dagger}. \tag{A9}$$

An arbitrary coin state ρ_{c}^{t} can be described with Pauli matrices $\{\mathbb{1}, \sigma_x, \sigma_y, \sigma_z\}$ by

$$\begin{aligned}\rho_{\mathrm{c}}^{t} &= \alpha_0 \mathbb{1} + \alpha_1\sigma_x + \alpha_2\sigma_y + \alpha_3\sigma_z \\ &= \begin{pmatrix} \alpha_0+\alpha_3 & \alpha_1 - i\alpha_2 \\ \alpha_1 + i\alpha_2 & \alpha_0 - \alpha_3 \end{pmatrix} \\ &= \begin{pmatrix} \frac{1}{2}+\alpha_3 & \alpha_1 - i\alpha_2 \\ \alpha_1 + i\alpha_2 & \frac{1}{2} - \alpha_3 \end{pmatrix}, \end{aligned} \tag{A10}$$

where $\alpha_0 = \frac{1}{2}$ satisfying $\mathrm{tr}(\rho) = 2\alpha_0 = 1$. Using the affine map approach [86], we represent $\hat{\mathcal{L}}$ as a matrix acting on the 2×2 ρ_{c}^t, which can be further expressed as a four-dimensional column vector $\boldsymbol{\alpha}_{\mathrm{c}}^t$ [87]:

$$\boldsymbol{\alpha}_{\mathrm{c}}^t = \begin{pmatrix} \frac{1}{2} \\ \alpha_1 \\ \alpha_2 \\ \alpha_3 \end{pmatrix}, \tag{A11}$$

where $\alpha_i = \frac{1}{2}\mathrm{tr}(\rho\sigma_i)$. Along this spirit, dynamic evolution of the density matrix of the coin can be expressed as

$$\boldsymbol{\alpha}_c^{\mathrm{f}} = \int \frac{dk}{2\pi} \prod_{t=1}^{T} \hat{\mathcal{L}}_t \boldsymbol{\alpha}_c^{\mathrm{in}}, \tag{A12}$$

where $\boldsymbol{\alpha}_c^{\mathrm{in}}$ and $\boldsymbol{\alpha}_c^{\mathrm{f}}$ correspond to ρ_c^{in} and ρ_c^{f}, respectively.

For $\hat{H}_{\mathrm{m}}$, we have

$$\begin{aligned} &\hat{H}_{\mathrm{m}} \rho_{\mathrm{c}}^t \hat{H}_{\mathrm{m}}^{\dagger} \\ &= \begin{pmatrix} \frac{1}{2} + \alpha_1 & (\alpha_3 + i\alpha_2)e^{-2ik} \\ (\alpha_3 - i\alpha_2)e^{2ik} & \frac{1}{2} - \alpha_1 \end{pmatrix} \\ &= \begin{pmatrix} \frac{1}{2} \\ \alpha_3 \cos 2k + \alpha_2 \sin 2k \\ -\alpha_2 \cos 2k + \alpha_3 \sin 2k \\ \alpha_1 \end{pmatrix}. \end{aligned} \tag{A13}$$

Then we can calculate $\hat{\mathcal{L}}^H$ by

$$\hat{\mathcal{L}}^H \begin{pmatrix} \frac{1}{2} \\ \alpha_1 \\ \alpha_2 \\ \alpha_3 \end{pmatrix} = \begin{pmatrix} \frac{1}{2} \\ \alpha_2 \sin 2k + \alpha_3 \cos 2k \\ -\alpha_2 \cos 2k + \alpha_3 \sin 2k \\ \alpha_1 \end{pmatrix} \tag{A14}$$

and obtain the expression of $\hat{\mathcal{L}}^H$ as

$$\hat{\mathcal{L}}^H = \begin{pmatrix} 1 & 0 & 0 & 0 \\ 0 & 0 & \sin 2k & \cos 2k \\ 0 & 0 & -\cos 2k & \sin 2k \\ 0 & 1 & 0 & 0 \end{pmatrix}. \tag{A15}$$

Similarly, the expression of $\hat{\mathcal{L}}^{\mathbb{1}}$ is

$$\hat{\mathcal{L}}^{\mathbb{1}} = \begin{pmatrix} 1 & 0 & 0 & 0 \\ 0 & \cos 2k & -\sin 2k & 0 \\ 0 & \sin 2k & \cos 2k & 0 \\ 0 & 0 & 0 & 1 \end{pmatrix}. \tag{A16}$$

3. Optimal coin sequence

The optimal coin sequence $\boldsymbol{C}_T$ maps any initial coin state $\rho_{\mathrm{c}}^{\mathrm{in}} = |\theta, \phi\rangle_{\mathrm{c}}^{\mathrm{in}}\langle\theta, \phi|$ to identity state $\rho_{\mathrm{c}}^{\mathrm{f}} = 1/2$. In the context of superoperator, we have the following definition of optimal coin sequence.

Definition 1 (Optimal coin sequence). A coin sequence $\boldsymbol{C}_T$ is the optimal sequence if its corresponding superoperators can transform $\boldsymbol{\alpha}_c^{\mathrm{in}}$ to $\boldsymbol{\alpha}_c^{\mathrm{f}}$, where

$$\boldsymbol{\alpha}_c^{\mathrm{in}} = \frac{1}{2}\begin{pmatrix} 1 \\ \cos\phi \sin\theta \\ \sin\phi \sin\theta \\ \cos\theta \end{pmatrix}, \quad \boldsymbol{\alpha}_c^{\mathrm{f}} = \frac{1}{2}\begin{pmatrix} 1 \\ 0 \\ 0 \\ 0 \end{pmatrix}. \tag{A17}$$

We first propose the following optimal coin sequence with one Hadamard operation.

Theorem 1. Given $l_{1,2} \in \mathbb{N}$, the coin sequence with $\boldsymbol{b} = 1^{\otimes l_1}01^{\otimes l_2}$ is optimal if l_1 and l_2 satisfy $l_1 \neq 0$ and $l_1 \neq l_2 + 1$.

Proof. Given an $l \in \mathbb{N}^+$, $\hat{\mathcal{L}}^{\mathbb{1}}$ has the property of

$$(\hat{\mathcal{L}}^{\mathbb{1}})^{\otimes l} = \begin{pmatrix} 1 & 0 & 0 & 0 \\ 0 & \cos(2lk) & -\sin(2lk) & 0 \\ 0 & \sin(2lk) & \cos(2lk) & 0 \\ 0 & 0 & 0 & 1 \end{pmatrix}. \tag{A18}$$

Then we calculate $\boldsymbol{\alpha}_c^{\mathrm{f}}$ by

$$\begin{aligned} \boldsymbol{\alpha}_c^{\mathrm{f}} &= \int_{-\pi}^{\pi} \frac{dk}{2\pi} (\hat{\mathcal{L}}^{\mathbb{1}})^{\otimes l_2} \hat{\mathcal{L}}^H (\hat{\mathcal{L}}^{\mathbb{1}})^{\otimes l_1} \boldsymbol{\alpha}_c^{\mathrm{in}} \\ &= \int_{-\pi}^{\pi} \frac{dk}{2\pi} \frac{1}{2} \begin{pmatrix} 1 \\ \alpha_1 \\ \alpha_2 \\ \alpha_3 \end{pmatrix}, \end{aligned} \tag{A19}$$

where

$$\begin{aligned} \alpha_1 =& \cos\theta \cos[2(l_2+1)k] \\ &+ \sin\phi \sin\theta \sin[2(l_2+1)k] \cos(2l_1k) \\ &+ \cos\phi \sin\theta \sin[2(l_2+1)k] \sin(2l_1k), \\ \alpha_2 =& \cos\theta \sin[2(l_2+1)k] \\ &- \sin\phi \sin\theta \cos[2(l_2+1)k] \cos(2l_1k) \\ &- \cos\phi \sin\theta \cos[2(l_2+1)k] \sin(2l_1k), \\ \alpha_3 =& \cos\phi \sin\theta \cos(2l_1k) - \sin\phi \sin\theta \sin(2l_1k). \end{aligned} \tag{A20}$$

The momentum integral for α_3 is under the condition $l_1 \neq 0$, and that of α_1 and α_2 are 0 as well under the condition $l_1 \neq l_2 + 1$. Then the coin sequence with $\boldsymbol{b} = 1^{\otimes l_1}01^{\otimes l_2}$ transforms $\boldsymbol{\alpha}_c^{\mathrm{in}}$ to $\boldsymbol{\alpha}_c^{\mathrm{f}}$, satisfying Definition 1, and is the optimal coin sequence. ■

We then propose another optimal coin sequence with two Hadamard operations.

Theorem 2. Given $l_{1,2,3} \in \mathbb{N}$, the coin sequence with $\boldsymbol{b} = 1^{\otimes l_1}01^{\otimes l_2}01^{\otimes l_3}$ is the optimal coin sequence if l_1, l_2, and l_3 satisfy $l_1 \neq l_2 + 1$, $l_1 \neq l_3 + 1$, $l_2 \pm l_1 \neq l_3$, and $l_2 + l_3 - l_1 \neq 2$.

Proof. $\boldsymbol{\alpha}_c^{\mathrm{f}}$ is calculated by

$$\begin{aligned} \boldsymbol{\alpha}_c^{\mathrm{f}} &= \int_{-\pi}^{\pi} \frac{dk}{2\pi} (\hat{\mathcal{L}}^{\mathbb{1}})^{\otimes l_3} \hat{\mathcal{L}}^H (\hat{\mathcal{L}}^{\mathbb{1}})^{\otimes l_2} \hat{\mathcal{L}}^H (\hat{\mathcal{L}}^{\mathbb{1}})^{\otimes l_1} \boldsymbol{\alpha}_c^{\mathrm{in}} \\ &= \int_{-\pi}^{\pi} \frac{dk}{2\pi} \frac{1}{2} \begin{pmatrix} 1 \\ \alpha_1 \\ \alpha_2 \\ \alpha_3 \end{pmatrix}, \end{aligned} \tag{A21}$$

TABLE I. Experimental settings of coin sequences $\boldsymbol{C}_T$ with coin sets $\{\hat{H}, \hat{\mathbb{1}}\}$ and $\{\hat{H}, \hat{F}\}$.

T	$\boldsymbol{C}_T$ with coin set $\{\hat{H}, \hat{\mathbb{1}}\}$	$\boldsymbol{C}_T$ with coin set $\{\hat{H}, \hat{F}\}$
3	$\{\hat{H}, \hat{H}, \hat{\mathbb{1}}\}$	$\{\hat{F}, \hat{F}, \hat{H}\}$
4	$\{\hat{H}, \hat{H}, \hat{\mathbb{1}}, \hat{\mathbb{1}}\}$	$\{\hat{H}, \hat{F}, \hat{H}, \hat{H}\}$
5	$\{\hat{H}, \hat{H}, \hat{\mathbb{1}}, \hat{\mathbb{1}}, \hat{\mathbb{1}}\}$	$\{\hat{H}, \hat{F}, \hat{H}, \hat{F}, \hat{F}\}$
6	$\{\hat{H}, \hat{H}, \hat{\mathbb{1}}, \hat{\mathbb{1}}, \hat{\mathbb{1}}, \hat{\mathbb{1}}\}$	$\{\hat{F}, \hat{H}, \hat{F}, \hat{H}, \hat{H}, \hat{F}\}$
7	$\{\hat{H}, \hat{H}, \hat{\mathbb{1}}, \hat{H}, \hat{\mathbb{1}}, \hat{\mathbb{1}}, \hat{\mathbb{1}}\}$	$\{\hat{H}, \hat{H}, \hat{F}, \hat{H}, \hat{F}, \hat{F}, \hat{H}\}$
8	$\{\hat{H}, \hat{H}, \hat{\mathbb{1}}, \hat{H}, \hat{\mathbb{1}}, \hat{\mathbb{1}}, \hat{\mathbb{1}}, \hat{\mathbb{1}}\}$	$\{\hat{H}, \hat{F}, \hat{F}, \hat{F}, \hat{F}, \hat{H}, \hat{F}, \hat{F}\}$
9	$\{\hat{H}, \hat{H}, \hat{\mathbb{1}}, \hat{H}, \hat{\mathbb{1}}, \hat{\mathbb{1}}, \hat{\mathbb{1}}, \hat{\mathbb{1}}, \hat{\mathbb{1}}\}$	$\{\hat{F}, \hat{H}, \hat{F}, \hat{F}, \hat{H}, \hat{H}, \hat{H}, \hat{H}, \hat{F}\}$
10	$\{\hat{H}, \hat{H}, \hat{\mathbb{1}}, \hat{H}, \hat{\mathbb{1}}, \hat{\mathbb{1}}, \hat{\mathbb{1}}, \hat{\mathbb{1}}, \hat{\mathbb{1}}, \hat{\mathbb{1}}\}$	$\{\hat{F}, \hat{F}, \hat{H}, \hat{H}, \hat{H}, \hat{F}, \hat{F}, \hat{F}, \hat{H}, \hat{H}\}$

with

$$\begin{aligned}
\alpha_1 =& \cos\theta \sin[2(l_2+1)k] \sin[2(l_3+1)k] \\
&- \sin\phi \sin\theta \{\cos(2l_1k) \cos[2(l_2+1)k] \sin[2(l_3+1)k] \\
&+ \sin(2l_1k) \cos[2(l_3+1)k]\} \\
&- \cos\phi \sin\theta \{\sin(2l_1k) \cos[2(l_2+1)k] \sin[2(l_3+1)k] \\
&- \cos(2l_1k) \cos[2(l_3+1)k]\}, \\
\alpha_2 =& -\cos\theta \sin[2(l_2+1)k] \cos[2(l_3+1)k] \\
&- \sin\phi \sin\theta \{\cos(2l_1k) \cos[2(l_2+1)k] \cos[2(l_3+1)k] \\
&+ \sin(2l_1k) \sin[2(l_3+1)k]\} \\
&- \cos\phi \sin\theta \{\sin(2l_1k) \cos[2(l_2+1)k] \cos[2(l_3+1)k] \\
&- \cos(2l_1k) \cos[2(l_3+1)k]\}, \\
\alpha_3 =& \cos\theta \cos[2(l_2+1)k] \\
&+ \sin\phi \sin\theta \cos(2l_1k) \sin[2(l_2+1)k] \\
&+ \cos\phi \sin\theta \sin(2l_1k) \sin[2(l_2+1)k]. \qquad \text{(A22)}
\end{aligned}$$

The momentum integral for α_3 is under the condition $l_1 \neq l_2+1$, and that of α_1 and α_2 are 0 under the conditions $l_2 \pm l_1 \neq l_3$, $l_2 + l_3 - l_1 \neq 2$, and $l_1 \neq l_3 + 1$. ■

The coin operation $\hat{C}_1$ at the first step ($T = 1$) is equivalent to changing the initial coin state so that we have the following corollary.

Corollary 1. Given $l_1, l_2, l_3 \in \mathbb{N}$ satisfying Theorem 1 and Theorem 2, the coin sequences with $\boldsymbol{b} = 01^{\otimes(l_1-1)}01^{\otimes l_2}$ and $\boldsymbol{b} = 01^{\otimes(l_1-1)}01^{\otimes l_2}01^{\otimes l_3}$ are the optimal sequences.

Note that optimal $\boldsymbol{b}$ in Theorem 1, Theorem 2, and Corollary 1 is not limited to generating the maximal entanglement step T, but also leads to MEG in the intermediate steps t if the corresponding sequence $\boldsymbol{b} = b_1 b_2 \cdots b_t$ fulfills the conditions in Theorem 1, Theorem 2, or Corollary 1. We experimentally set the coin sequences $\boldsymbol{C}_T$ according to Corollary 1; they are listed in Table I.

APPENDIX B: GENERALIZED ELEPHANT QUANTUM WALK

In this section, we briefly introduce the gEQW in Refs. [56,59]. The main difference between the Hadamard QW and the gEQW is the shift operator in Eq. (8). The probability of Δ_t is determined by the discrete version of the q-exponential distribution in $[1, T]$ as

$$\Pr(\Delta_t) = e_q^{\Delta_t} = \tau_t [1 - (1-q)\Delta_t]^{1/1-q}, \qquad \text{(B1)}$$

with τ_t being a time-dependent normalization factor. The support of function Eq. (B1) is given by

$$\text{supp}[e_q(x)] = \begin{cases} [0, \frac{1}{1-q}] & q \leqslant 1, \\ [0, \infty] & q > 1. \end{cases} \qquad \text{(B2)}$$

When $q = \frac{1}{2}$, we obtain $\Delta_t \leqslant 2$ with probability distributions $\Pr(\Delta_t = 1) = 1$ and $\Pr(\Delta_t = 2) = 0$, which is the Hadamard QW; when $q \to 1$, we obtain a decreasing exponential $\Pr(\Delta_t) = \tau_t e^{-\Delta_t}$; and when $q \to \infty$, we obtain a uniform distribution $\Pr(\Delta_t) = \frac{1}{T}$.

The QWs with the optimal coin sequence in Corollary 1 are equivalent to the gEQW, i.e., $\boldsymbol{b} = 01^{\otimes(l_1-1)}01^{\otimes l_2}$ corresponds to a two-step gEQW with $\Delta_1 = l_1$ and $\Delta_2 = l_2 + 1$, and $\boldsymbol{b} = 01^{\otimes(l_1-1)}01^{\otimes l_2}01^{\otimes l_3}$ corresponds to a three-step gEQW with $\Delta_1 = l_1$, $\Delta_2 = l_2 + 1$, and $\Delta_3 = l_3 + 1$. In this sense, QWs with the optimal coin sequence in Corollary 1 are gEQW with specific shift-operator configurations, for which the maximal entanglement generation in the asymptotic approach has been reported [59].

APPENDIX C: MORE EXPERIMENTAL RESULTS

The reconstructed $\chi_{\boldsymbol{C}_T}^{\text{exp}}$ with the coin sequences in Table Iare shown in Eq. (C1), according to which we calculate the process fidelities $\mathcal{F}_{\boldsymbol{C}_3} = 0.9976 \pm 0.0003$, $\mathcal{F}_{\boldsymbol{C}_4} = 0.9955 \pm 0.0016$, $\mathcal{F}_{\boldsymbol{C}_5} = 0.9939 \pm 0.0011$, $\mathcal{F}_{\boldsymbol{C}_6} = 0.9951 \pm 0.0009$, $\mathcal{F}_{\boldsymbol{C}_7} = 0.9975 \pm 0.0004$, $\mathcal{F}_{\boldsymbol{C}_8} = 0.9885 \pm 0.0015$, $\mathcal{F}_{\boldsymbol{C}_9} = 0.9968 \pm 0.0004$, and $\mathcal{F}_{\boldsymbol{C}_{10}} = 0.9980 \pm 0.0003$. The geometric representations of the reconstructed $\chi_{\boldsymbol{C}_T}^{\text{exp}}$ with coin sets $\{\hat{H}, \hat{\mathbb{1}}\}$ and $\{\hat{H}, \hat{F}\}$ at $T = 3$, 5, 7, and 9 are shown in Fig. 6. The reconstructed $\chi_{\boldsymbol{C}_T}^{\text{exp}}$ are as

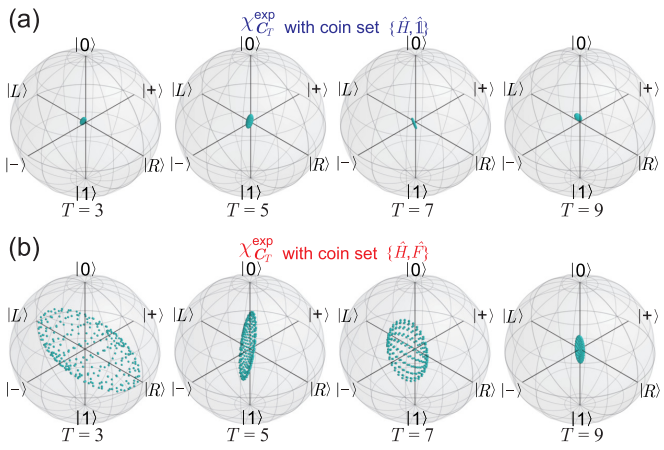

FIG. 6. (a) Geometric representation of the reconstructed $\chi_{\boldsymbol{C}_T}^{\text{exp}}$ with the coin set $\{\hat{H}, \hat{\mathbb{1}}\}$ at $T = 3$, 5, 7, and 9. (b) Geometric representation of the reconstructed $\chi_{\boldsymbol{C}_T}^{\text{exp}}$ with the coin set $\{\hat{H}, \hat{F}\}$ at $T = 3$, 5, 7, and 9.

TABLE II. Comparison of performances of entanglement generation with different coin sequences.

	Steps[a]	Independence[b]	Number of operations[c]	Technique[d]	Figure of merit	Experimental demonstrations
This work	$T \geqslant 3$	Yes	$N_c = 1$; $N_s = 1$	Annealing and Fourier analysis	$\mathcal{F}_{\boldsymbol{C}_T}$	Linear optics (this work)
Vieira *et al.* [41]	$T \to \infty$	Yes	$N_c = 2$; $N_s = 1$	Disorder	$\langle \mathcal{S}_{\mathrm{E}} \rangle$	Linear optics (Wang *et al.* [53])
Govind *et al.* [66]	$T = 3, 5$	Partially[e]	$N_c = 2$; $N_s = 1$	Parrondo sequences	$\langle \mathcal{S}_{\mathrm{E}} \rangle$	None
Gratsea *et al.* [64]	$T \geqslant 1$	No	Full set of SU(2) coins; $N_s = 1$	Basin hopping	$\langle \mathcal{S}_{\mathrm{E}} \rangle$ and Inverse participation ration	Linear optics (Tao *et al.* [54])
Gratsea *et al.* [65]	None	Partially[f]	$N_c = 2$; $N_s = 1$	Reinforcement learning	$\langle \mathcal{S}_{\mathrm{E}} \rangle$	None
Zhang *et al.* [55]	Odd steps	No	$N_c = 2$; $N_s = 1$	Numerical	$\langle \mathcal{S}_{\mathrm{E}} \rangle$	Linear optics (Zhang *et al.* [55])
Pires *et al.* [56]; Naves *et al.* [59]	$T \to \infty$	Almost	$N_c = 1$; $N_s \to \infty$	q-exponential distribution	$\langle \mathcal{S}_{\mathrm{E}} \rangle$	Our demonstration corresponds to a specific case of this protocol

[a]The steps that the average von Neumann entropy $\langle \mathcal{S}_{\mathrm{E}} \rangle = 1$ or the process fidelity $\mathcal{F}_{\boldsymbol{C}_T} = 1$ is fulfilled.
[b]The independence of the initial coin state $|\theta, \phi\rangle_{\mathrm{c}}^{\mathrm{in}} = \cos(\theta/2)|0\rangle_{\mathrm{c}} + e^{i\phi} \sin(\theta/2)|1\rangle_{\mathrm{c}}$.
[c]The number of coin operations N_c in the coin sequence $\boldsymbol{C}_T$ and the number of shift operations N_s.
[d]Techniques and algorithms to determine the coin set or the coin sequence $\boldsymbol{C}_T$.
[e]Independent of ϕ.
[f]Universal sequence: independent of θ when $\phi = 0$. Optimal sequence: dependent on θ and ϕ.

follows:

$$\chi_{\boldsymbol{C}_3}^{\mathrm{exp}} = \begin{pmatrix} 0.2580 - 0.0000i & 0.0013 - 0.0003i & -0.0135 - 0.0118i & 0.0050 - 0.0006i \\ 0.0013 + 0.0003i & 0.2320 - 0.0000i & -0.0084 + 0.0020i & -0.0163 + 0.0042i \\ -0.0135 + 0.0118i & -0.0084 - 0.0020i & 0.2520 - 0.0000i & 0.0074 + 0.0046i \\ 0.0050 + 0.0006i & -0.0163 - 0.0042i & 0.0074 - 0.0046i & 0.2579 - 0.0000i \end{pmatrix},$$

$$\chi_{\boldsymbol{C}_4}^{\mathrm{exp}} = \begin{pmatrix} 0.2461 - 0.0000i & -0.0046 + 0.0056i & 0.0101 + 0.0059i & 0.0028 - 0.0145i \\ -0.0046 - 0.0056i & 0.2518 - 0.0000i & -0.0082 - 0.0092i & -0.0327 + 0.0011i \\ 0.0101 - 0.0059i & -0.0082 + 0.0092i & 0.2408 - 0.0000i & 0.0062 - 0.0037i \\ 0.0028 + 0.0145i & -0.0327 - 0.0011i & 0.0062 + 0.0037i & 0.2613 - 0.0000i \end{pmatrix},$$

$$\chi_{\boldsymbol{C}_5}^{\mathrm{exp}} = \begin{pmatrix} 0.2441 - 0.0000i & 0.0165 + 0.0087i & 0.0071 - 0.0204i & 0.0133 + 0.0021i \\ 0.0165 - 0.0087i & 0.2524 - 0.0000i & -0.0093 + 0.0090i & -0.0366 - 0.0049i \\ 0.0071 + 0.0204i & -0.0093 - 0.0090i & 0.2405 - 0.0000i & -0.0001 + 0.0054i \\ 0.0133 - 0.0021i & -0.0366 + 0.0049i & -0.0001 - 0.0054i & 0.2630 - 0.0000i \end{pmatrix},$$

$$\chi_{\boldsymbol{C}_6}^{\mathrm{exp}} = \begin{pmatrix} 0.2728 - 0.0000i & -0.0247 - 0.0021i & -0.0038 - 0.0147i & -0.0046 - 0.0035i \\ -0.0247 + 0.0021i & 0.2594 - 0.0000i & 0.0099 + 0.0002i & -0.0138 + 0.0025i \\ -0.0038 + 0.0147i & 0.0099 - 0.0002i & 0.2298 - 0.0000i & 0.0061 + 0.0188i \\ -0.0046 + 0.0035i & -0.0138 - 0.0025i & 0.0061 - 0.0188i & 0.2380 - 0.0000i \end{pmatrix},$$

$$\chi_{\boldsymbol{C}_7}^{\mathrm{exp}} = \begin{pmatrix} 0.2333 - 0.0000i & 0.0051 - 0.0009i & 0.0005 - 0.0085i & -0.0044 - 0.0086i \\ 0.0051 + 0.0009i & 0.2634 - 0.0000i & 0.0049 - 0.0041i & -0.0191 + 0.0035i \\ 0.0005 + 0.0085i & 0.0049 + 0.0041i & 0.2642 - 0.0000i & -0.0040 + 0.0050i \\ -0.0044 + 0.0086i & -0.0191 - 0.0035i & -0.0040 - 0.0050i & 0.2392 - 0.0000i \end{pmatrix},$$

$$\chi_{\boldsymbol{C}_8}^{\mathrm{exp}} = \begin{pmatrix} 0.2327 - 0.0000i & 0.0146 + 0.0030i & 0.0267 - 0.0002i & 0.0214 - 0.0324i \\ 0.0146 - 0.0030i & 0.2353 - 0.0000i & 0.0191 + 0.0321i & 0.0211 - 0.0020i \\ 0.0267 + 0.0002i & 0.0191 - 0.0321i & 0.2461 - 0.0000i & 0.0038 + 0.0123i \\ 0.0214 + 0.0324i & 0.0211 + 0.0020i & 0.0038 - 0.0123i & 0.2859 - 0.0000i \end{pmatrix},$$

$$\chi_{C_9}^{\exp} = \begin{pmatrix} 0.2563 - 0.0000i & -0.0141 + 0.0002i & -0.0144 + 0.0135i & 0.0103 - 0.0064i \\ -0.0141 - 0.0002i & 0.2480 - 0.0000i & -0.0112 + 0.0124i & 0.0110 + 0.0101i \\ -0.0144 - 0.0135i & -0.0112 - 0.0124i & 0.2524 - 0.0000i & -0.0066 + 0.0063i \\ 0.0103 + 0.0064i & 0.0110 - 0.0101i & -0.0066 - 0.0063i & 0.2433 - 0.0000i \end{pmatrix},$$

$$\chi_{C_{10}}^{\exp} = \begin{pmatrix} 0.2596 - 0.0000i & -0.0011 - 0.0055i & 0.0026 - 0.0127i & -0.0037 + 0.0004i \\ -0.0011 + 0.0055i & 0.2384 - 0.0000i & -0.0031 - 0.0117i & -0.0156 - 0.0060i \\ 0.0026 + 0.0127i & -0.0031 + 0.0117i & 0.2516 - 0.0000i & -0.0036 + 0.0065i \\ -0.0037 - 0.0004i & -0.0156 + 0.0060i & -0.0036 - 0.0065i & 0.2503 - 0.0000i \end{pmatrix}. \quad \text{(C1)}$$

APPENDIX D: A COMPARISON OF OUR COIN SEQUENCE WITH THE OTHER COIN SEQUENCES

In the context of MEG, a comparison of our coin sequence $\boldsymbol{C}_T$ with the other coin sequences including the disordered coin sequence [41], Parrondo sequences [66], three coin sequences proposed by Gratsea *et al.* [64,65], the position-inhomogeneous coin sequence [55], and the gEQW with disordered shift operations [56,59] is shown in Table II.

[1] Y. Aharonov, L. Davidovich, and N. Zagury, Quantum random walks, Phys. Rev. A **48**, 1687 (1993).

[2] J Kempe, Quantum random walks: An introductory overview, Contemp. Phys. **44**, 307 (2003).

[3] A. M. Childs and J. Goldstone, Spatial search by quantum walk, Phys. Rev. A **70**, 022314 (2004).

[4] A. M. Childs, Universal computation by Quantum Walk, Phys. Rev. Lett. **102**, 180501 (2009).

[5] N. B. Lovett, S. Cooper, M. Everitt, M. Trevers, and V. Kendon, Universal quantum computation using the discrete-time quantum walk, Phys. Rev. A **81**, 042330 (2010).

[6] A. M. Childs, D. Gosset, and Z. Webb, Universal computation by multiparticle quantum walk, Science **339**, 791 (2013).

[7] A. Schreiber, A. Gábris, P. P. Rohde, K. Laiho, M. Štefaňák, V. Potoček, C. Hamilton, I. Jex, and C. Silberhorn, A 2D quantum walk simulation of two-particle dynamics, Science **336**, 55 (2012).

[8] P. Kurzyński and A. Wójcik, Quantum Walk as a Generalized Measuring Device, Phys. Rev. Lett. **110**, 200404 (2013).

[9] Z. Bian, J. Li, H. Qin, X. Zhan, R. Zhang, B. C. Sanders, and P. Xue, Realization of Single-Qubit Positive-Operator-Valued Measurement via a One-Dimensional Photonic Quantum Walk, Phys. Rev. Lett. **114**, 203602 (2015).

[10] Y.-Y. Zhao, N.-K. Yu, P. Kurzyński, G.-Y. Xiang, C.-F. Li, and G.-C. Guo, Experimental realization of generalized qubit measurements based on quantum walks, Phys. Rev. A **91**, 042101 (2015).

[11] T. Kitagawa, M. S. Rudner, E. Berg, and E. Demler, Exploring topological phases with quantum walks, Phys. Rev. A **82**, 033429 (2010).

[12] J. K. Asbóth, Symmetries, topological phases, and bound states in the one-dimensional quantum walk, Phys. Rev. B **86**, 195414 (2012).

[13] T. Kitagawa, M. A. Broome, A. Fedrizzi, M. S. Rudner, E. Berg, I. Kassal, A. Aspuru-Guzik, E. Demler, and A. G. White, Observation of topologically protected bound states in photonic quantum walks, Nat. Commun. **3**, 882 (2012).

[14] L. Xiao, X. Zhan, Z. H. Bian, K. K. Wang, X. Zhang, X. P. Wang, J. Li, K. Mochizuki, D. Kim, N. Kawakami, W. Yi, H. Obuse, B. C. Sanders, and P. Xue, Observation of topological edge states in parity–time-symmetric quantum walks, Nat. Phys. **13**, 1117 (2017).

[15] X. Wang, L. Xiao, X. Qiu, K. Wang, W. Yi, and P. Xue, Detecting topological invariants and revealing topological phase transitions in discrete-time photonic quantum walks, Phys. Rev. A **98**, 013835 (2018).

[16] K. Wang, X. Qiu, L. Xiao, X. Zhan, Z. Bian, W. Yi, and P. Xue, Simulating Dynamic Quantum Phase Transitions in Photonic Quantum Walks, Phys. Rev. Lett. **122**, 020501 (2019).

[17] X.-Y. Xu, Q.-Q. Wang, S.-J. Tao, W.-W. Pan, Z. Chen, M. Jan, Y.-T. Zhan, K. Sun, J.-S. Xu, Y.-J. Han, C.-F. Li, and G.-C. Guo, Experimental classification of quenched quantum walks by dynamical chern number, Phys. Rev. Res. **1**, 033039 (2019).

[18] J. Wu, W.-W. Zhang, and B. C. Sanders, Topological quantum walks: Theory and experiments, Front. Phys. **14**, 61301 (2019).

[19] I. Carneiro, M. Loo, X. Xu, M. Girerd, V. Kendon, and P. L. Knight, Entanglement in coined quantum walks on regular graphs, New J. Phys. **7**, 156 (2005).

[20] G. Abal, R. Siri, A. Romanelli, and R. Donangelo, Quantum walk on the line: Entanglement and nonlocal initial conditions, Phys. Rev. A **73**, 042302 (2006).

[21] M. Annabestani, M. R. Abolhasani, and G. Abal, Asymptotic entanglement in 2D quantum walks, J. Phys. A: Math. Theor. **43**, 075301 (2010).

[22] C. Di Franco, M. Mc Gettrick, and Th. Busch, Mimicking the Probability Distribution of a Two-Dimensional Grover Walk with a Single-Qubit Coin, Phys. Rev. Lett. **106**, 080502 (2011).

[23] R. Horodecki, P. Horodecki, M. Horodecki, and K. Horodecki, Quantum entanglement, Rev. Mod. Phys. **81**, 865 (2009).

[24] M. Erhard, M. Krenn, and A. Zeilinger, Advances in high-dimensional quantum entanglement, Nat. Rev. Phys. **2**, 365 (2020).

[25] K.-C. Ha, Separability of qubit-qudit quantum states with strong positive partial transposes, Phys. Rev. A **87**, 024301 (2013).

[26] M.-J. Zhao, T. Ma, S.-M. Fei, and Z.-X. Wang, Inequalities detecting quantum entanglement for $2 \bigotimes d$ systems, Phys. Rev. A **83**, 052120 (2011).

[27] L. Chen and D. Ž. Đoković, Qubit-qudit states with positive partial transpose, Phys. Rev. A **86**, 062332 (2012).

[28] N. Johnston, Separability from spectrum for qubit-qudit states, Phys. Rev. A **88**, 062330 (2013).

[29] S.-Q. Shen, J.-M. Liang, M. Li, J. Yu, and S.-M. Fei, Nonlinear improvement of qubit-qudit entanglement witnesses, Phys. Rev. A **101**, 012312 (2020).

[30] E. Gerjuoy, Lower bound on entanglement of formation for the qubit-qudit system, Phys. Rev. A **67**, 052308 (2003).

[31] F. Lastra, C. E. López, L. Roa, and J. C. Retamal, Entanglement of formation for a family of $(2 \bigotimes d)$-dimensional systems, Phys. Rev. A **85**, 022320 (2012).

[32] J. Dajka and J. Łuczka, Origination and survival of qudit-qudit entanglement in open systems, Phys. Rev. A **77**, 062303 (2008).

[33] T. Giordani, L. Innocenti, A. Suprano, E. Polino, M. Paternostro, N. Spagnolo, F. Sciarrino, and A. Ferraro, Entanglement transfer, accumulation and retrieval via quantum-walk-based qubit–qudit dynamics, New J. Phys. **23**, 023012 (2021).

[34] F. Mintert, M. Kuś, and A. Buchleitner, Concurrence of Mixed Bipartite Quantum States in Arbitrary Dimensions, Phys. Rev. Lett. **92**, 167902 (2004).

[35] K. Chen, S. Albeverio, and S.-M. Fei, Concurrence of Arbitrary Dimensional Bipartite Quantum States, Phys. Rev. Lett. **95**, 040504 (2005).

[36] M.-J. Zhao, X.-N. Zhu, S.-M. Fei, and X. Li-Jost, Lower bound on concurrence and distillation for arbitrary-dimensional bipartite quantum states, Phys. Rev. A **84**, 062322 (2011).

[37] S. Vinjanampathy and A. R. P. Rau, Quantum discord for qubit–qudit systems, J. Phys. A: Math. Theor. **45**, 095303 (2012).

[38] D. Girolami and G. Adesso, Observable Measure of Bipartite Quantum Correlations, Phys. Rev. Lett. **108**, 150403 (2012).

[39] Z. Ma, Z. Chen, F. F. Fanchini, and S.-M. Fei, Quantum discord for $d \otimes 2$ systems, Sci. Rep. **5**, 10262 (2015).

[40] C. M. Chandrashekar, Disorder induced localization and enhancement of entanglement in one- and two-dimensional quantum walks, arXiv:1212.5984.

[41] R. Vieira, E. P. M. Amorim, and G. Rigolin, Dynamically Disordered Quantum Walk as a Maximal Entanglement Generator, Phys. Rev. Lett. **111**, 180503 (2013).

[42] R. Vieira, E. P. M. Amorim, and G. Rigolin, Entangling power of disordered quantum walks, Phys. Rev. A **89**, 042307 (2014).

[43] S. Salimi and R. Yosefjani, Asymptotic entanglement in 1D quantum walks with a time-dependent coined, Int. J. Mod. Phys. B **26**, 1250112 (2012).

[44] P. P. Rohde, G. K. Brennen, and A. Gilchrist, Quantum walks with memory provided by recycled coins and a memory of the coin-flip history, Phys. Rev. A **87**, 052302 (2013).

[45] M. Montero, Classical-like behavior in quantum walks with inhomogeneous, time-dependent coin operators, Phys. Rev. A **93**, 062316 (2016).

[46] G. Di Molfetta and F. Debbasch, Discrete-time quantum walks in random artificial gauge fields, Quantum Stud.: Math. Found. **3**, 293 (2016).

[47] M. Zeng and E. H. Yong, Discrete-time quantum walk with phase disorder: Localization and entanglement entropy, Sci. Rep. **7**, 12024 (2017).

[48] A. C. Orthey and E. P. M. Amorim, Weak disorder enhancing the production of entanglement in quantum walks, Braz. J. Phys. **49**, 595 (2019).

[49] S. Singh, R. Balu, R. Laflamme, and C. M. Chandrashekar, Accelerated quantum walk, two-particle entanglement generation and localization, J. Phys. Commun. **3**, 055008 (2019).

[50] A. R. C. Buarque and W. S. Dias, Aperiodic space-inhomogeneous quantum walks: Localization properties, energy spectra, and enhancement of entanglement, Phys. Rev. E **100**, 032106 (2019).

[51] M. A. Pires and S. M. Duarte Queirós, Negative correlations can play a positive role in disordered quantum walks, Sci. Rep. **11**, 4527 (2021).

[52] A. Laneve, F. Nosrati, A. Geraldi, K. Mahdavipour, F. Pegoraro, M. K. Shadfar, R. Lo Franco, and P. Mataloni, Enhancing nonclassical bosonic correlations in a quantum walk network through experimental control of disorder, Phys. Rev. Res. **3**, 033235 (2021).

[53] Q.-Q. Wang, X.-Y. Xu, W.-W. Pan, K. Sun, J.-S. Xu, G. Chen, Y.-J. Han, C.-F. Li, and G.-C. Guo, Dynamic-disorder-induced enhancement of entanglement in photonic quantum walks, Optica **5**, 1136 (2018).

[54] S.-J. Tao, Q.-Q. Wang, Z. Chen, W.-W. Pan, S. Yu, G. Chen, X.-Y. Xu, Y.-J. Han, C.-F. Li, and G.-C. Guo, Experimental optimal generation of hybrid entangled states in photonic quantum walks, Opt. Lett. **46**, 1868 (2021).

[55] R. Zhang, R. Yang, J. Guo, C.-W. Sun, J.-C. Duan, H. Zhou, Z. Xie, P. Xu, Y.-X. Gong, and S.-N. Zhu, Maximal coin-walker entanglement in a ballistic quantum walk, Phys. Rev. A **105**, 042216 (2022).

[56] M. A. Pires, G. D. Molfetta, and S. M. D. Queirós, Multiple transitions between normal and hyperballistic diffusion in quantum walks with time-dependent jumps, Sci. Rep. **9**, 19292 (2019).

[57] P. Sen, Scaling and crossover behaviour in a truncated long range quantum walk, Phys. A (Amsterdam, Neth.) **545**, 123529 (2020).

[58] M. A. Pires and S. M. D. Queirós, Quantum walks with sequential aperiodic jumps, Phys. Rev. E **102**, 012104 (2020).

[59] C. B. Naves, M. A. Pires, D. O. Soares-Pinto, and S. M. D. Queirós, Enhancing entanglement with the generalized elephant quantum walk from localized and delocalized states, Phys. Rev. A **106**, 042408 (2022).

[60] M. A. Pires and S. M. D. Queirós, Parrondo's paradox in quantum walks with time-dependent coin operators, Phys. Rev. E **102**, 042124 (2020).

[61] M. Jan, Q.-Q. Wang, X.-Y. Xu, W.-W. Pan, Z. Chen, Y.-J. Han, C.-F. Li, G.-C. Guo, and D. Abbott, Experimental realization of Parrondo's paradox in 1D quantum walks, Adv. Quantum Technol. **3**, 1900127 (2020).

[62] Z. Walczak and J. H. Bauer, Parrondo's paradox in quantum walks with deterministic aperiodic sequence of coins, Phys. Rev. E **104**, 064209 (2021).

[63] Z. Walczak and J. H. Bauer, Parrondo's paradox in quantum walks with three coins, Phys. Rev. E **105**, 064211 (2022).

[64] A. Gratsea, M. Lewenstein, and A. Dauphin, Generation of hybrid maximally entangled states in a one-dimensional quantum walk, Quantum Sci. Technol. **5**, 025002 (2020).

[65] A. Gratsea, F. Metz, and T. Busch, Universal and optimal coin sequences for high entanglement generation in 1D discrete time quantum walks, J. Phys. A: Math. Theor. **53**, 445306 (2020).

[66] D. K. Panda, B. V. Govind, and C. Benjamin, Generating highly entangled states via discrete-time quantum walks with Parrondo sequences, Phys. A (Amsterdam, Neth.) **608**, 128256 (2022).

[67] C. H. Bennett, H. J. Bernstein, S. Popescu, and B. Schumacher, Concentrating partial entanglement by local operations, Phys. Rev. A **53**, 2046 (1996).

[68] M. A. Nielsen and I. L. Chuang, *Quantum Computation and Quantum Information: 10th Anniversary Edition* (Cambridge University, New York, 2011).

[69] I. Bongioanni, L. Sansoni, F. Sciarrino, G. Vallone, and P. Mataloni, Experimental quantum process tomography of non-trace-preserving maps, Phys. Rev. A **82**, 042307 (2010).

[70] M. M. Wilde, *Quantum Information Theory*, 2nd ed. (Cambridge University, Cambridge, England, 2017).

[71] C. Tsallis, Nonadditive entropy and nonextensive statistical mechanics-an overview after 20 years, Braz. J. Phys. **39**, 337 (2009).

[72] M. A. Broome, A. Fedrizzi, B. P. Lanyon, I. Kassal, A. Aspuru-Guzik, and A. G. White, Discrete Single-Photon Quantum Walks with Tunable Decoherence, Phys. Rev. Lett. **104**, 153602 (2010).

[73] P. Xue, H. Qin, B. Tang, and B. C. Sanders, Observation of quasiperiodic dynamics in a one-dimensional quantum walk of single photons in space, New J. Phys. **16**, 053009 (2014).

[74] P. Xue, R. Zhang, H. Qin, X. Zhan, Z. H. Bian, J. Li, and B. C. Sanders, Experimental Quantum-Walk Revival with a Time-Dependent Coin, Phys. Rev. Lett. **114**, 140502 (2015).

[75] J.-Y. Li, X.-X. Fang, T. Zhang, G. N. M. Tabia, H. Lu, and Y.-C. Liang, Activating hidden teleportation power: Theory and experiment, Phys. Rev. Res. **3**, 023045 (2021).

[76] Q.-M. Ding, X.-X. Fang, X. Yuan, T. Zhang, and H. Lu, Efficient estimation of multipartite quantum coherence, Phys. Rev. Res. **3**, 023228 (2021).

[77] T. Zhang, J. Sun, X.-X. Fang, X.-M. Zhang, X. Yuan, and H. Lu, Experimental Quantum State Measurement with Classical Shadows, Phys. Rev. Lett. **127**, 200501 (2021).

[78] G. Martín-Vázquez and J. Rodríguez-Laguna, Optimizing the spatial spread of a quantum walk, Phys. Rev. A **102**, 022223 (2020).

[79] S. Havlin and D. Ben-Avraham, Diffusion in disordered media, Adv. Phys. **36**, 695 (1987).

[80] C. M. Chandrashekar, R. Srikanth, and R. Laflamme, Optimizing the discrete time quantum walk using a SU(2) coin, Phys. Rev. A **77**, 032326 (2008).

[81] V. Kendon and B. Tregenna, Decoherence can be useful in quantum walks, Phys. Rev. A **67**, 042315 (2003).

[82] O. Maloyer and V. Kendon, Decoherence versus entanglement in coined quantum walks, New J. Phys. **9**, 87 (2007).

[83] A. Geraldi, A. Laneve, L. D. Bonavena, L. Sansoni, J. Ferraz, A. Fratalocchi, F. Sciarrino, Á. Cuevas, and P. Mataloni, Experimental Investigation of Superdiffusion via Coherent Disordered Quantum Walks, Phys. Rev. Lett. **123**, 140501 (2019).

[84] A. Geraldi, S. De, A. Laneve, S. Barkhofen, J. Sperling, P. Mataloni, and C. Silberhorn, Transient subdiffusion via disordered quantum walks, Phys. Rev. Res. **3**, 023052 (2021).

[85] A. Nayak and A. Vishwanath, Quantum walk on the line, arXiv:quant-ph/0010117.

[86] T. A. Brun, H. A. Carteret, and A. Ambainis, Quantum walks driven by many coins, Phys. Rev. A **67**, 052317 (2003).

[87] M. Annabestani, S. J. Akhtarshenas, and M. R. Abolhassani, Decoherence in a one-dimensional quantum walk, Phys. Rev. A **81**, 032321 (2010).

[88] M. Hinarejos, C. Di Franco, A. Romanelli, and A. Pérez, Chirality asymptotic behavior and non-Markovianity in quantum walks on a line, Phys. Rev. A **89**, 052330 (2014).